Coulomb-enhanced superconducting pair correlations and paired-electron liquid in the frustrated quarter-filled band

Niladri Gomes,[1] W. Wasanthi De Silva,[2] Tirthankar Dutta,[1] R. Torsten Clay,[2,*] and S. Mazumdar[1,†]

[1]*Department of Physics, University of Arizona, Tucson, Arizona 85721, USA*

[2]*Department of Physics & Astronomy and HPC² Center for Computational Sciences, Mississippi State, Mississippi 39762, USA*

(Received 1 July 2015; revised manuscript received 11 March 2016; published 7 April 2016)

A necessary condition for superconductivity (SC) driven by electron correlations is that electron-electron (e-e) interactions enhance superconducting pair-pair correlations, relative to the noninteracting limit. We report high-precision numerical calculations of the ground state on four different finite lattices of up to 100 sites within the frustrated two-dimensional (2D) Hubbard Hamiltonian for a wide range of carrier concentration ρ ($0 < \rho < 1$). The average long-range pair-pair correlation for each cluster is enhanced by Hubbard U only for $\rho \approx 0.5$. At all other fillings e-e interactions mostly suppress pair correlations. Our work provides a key ingredient to the mechanism of SC in the 2D organic charge-transfer solids and many other unconventional superconductors with frustrated crystal lattices and $\rho \simeq 0.5$.

DOI: 10.1103/PhysRevB.93.165110

I. INTRODUCTION

The possibility that electron-electron (e-e) interactions drive superconductivity (SC) in correlated-electron systems has been intensely investigated. The minimal requirements for a complete theory are, (i) superconducting pair correlations are enhanced by e-e interactions, and (ii) pair correlations are long range. For moderate to large e-e interactions, pair correlations are perhaps best calculated numerically, which can be done only for finite clusters. The simplest model incorporating e-e interactions is the Hubbard model,

$$H = -\sum_{\langle ij\rangle,\sigma} t_{ij} B_{i,j,\sigma} + U \sum_i n_{i,\uparrow} n_{i,\downarrow} + \frac{1}{2} \sum_{\langle ij\rangle} V_{ij} n_i n_j. \quad (1)$$

In Eq. (1), $B_{i,j,\sigma} = (c^\dagger_{i,\sigma} c_{j,\sigma} + \text{H.c.})$ where $c^\dagger_{i,\sigma}$ creates an electron of spin σ on site i. U and V_{ij} are on-site and nearest-neighbor (n.n.) Coulomb interactions, respectively. Numerical calculations within Eq. (1) have failed to find enhancement of pair-pair correlations relative to the noninteracting model without making assumptions regarding the wave function [1]. Indeed, quantum Monte Carlo calculations on finite lattices find suppression of pair correlations by U [2–6].

It has been surmised that correlated-electron SC evolves upon doping a spin-gapped semiconductor, as in toy models consisting of weakly coupled even-leg ladders [7,8]. Finding realistic 2D models with spin-gap (SG) and enhanced-pair correlations remains challenging. Here we demonstrate from explicit numerical calculations on frustrated 2D lattices enhanced-pair correlations evolving from a spin-gapped state at a carrier density $\rho \simeq 0.5$, far from the region most heavily investigated ($0.7 < \rho < 1.0$). We point out the strong relevance of the resulting theoretical picture to real materials, in particular the 2D charge-transfer solids (CTS) superconductors, which were discovered before the high T_c cuprates [9] but are still not understood.

There occurs an effective e-e attraction uniquely at $\rho = 0.5$, driven by charge-spin-lattice coupling. Consider the four-atom dimerized "molecule" of Fig. 1(a), with two strong intradimer bonds and one electron on each dimer. In the absence of the interdimer bond, the electron density is homogeneous. As this bond is switched on, there is net migration of charge to the two center atoms, due to the attractive antiferromagnetic spin-coupling [10]. Charge migration is enhanced by electron-phonon (e-p) interactions [10,11]. The effective attraction is stronger than that near $\rho \sim 1$, where charge migration is not possible, with the neighboring sites already occupied. The charge-ordering (CO) of Fig. 1(a) in the spin-singlet state persists in the thermodynamic limit in one dimension (1D) $\rho = 0.5$, where for $V < V_c(U)$ e-e and e-p couplings act cooperatively [11] to give the spin-Peierls states of Figs. 1(b) and 1(c). The spin-Peierls state at $\rho = 0.5$ is a *paired-electron crystal* (PEC), in which singlet-coupled n.n. singly occupied sites are separated by pairs of vacancies. Similar PECs occur in the zigzag ladder [Fig. 1(d)] [12] and in the anisotropic triangular lattice [Fig. 1(e)] [10]. We have not found the PEC [10] at any other ρ. *This is expected, as only at* $\rho = 0.5$ *the PEC is commensurate.*

Based on a valence bond (VB) perspective similar to Anderson's resonating valence bond [13] approach to the nearly $\rho = 1$ limit, we posit that SC is achieved in $\rho \simeq 0.5$ upon destabilization of the PEC, either due to increased frustration or very weak doping. The PEC wave function is dominated by covalent VB diagrams with periodic arrangement of the n.n. singlet bonds. Close to the PEC we anticipate the wave function to continue to be dominated by VB diagrams with n.n. singlet bonds, except that the arrangement of the bonds is no longer periodic. One such diagram is shown in Fig. 1(f)(i). Within Eq. (1), pairs of VB diagrams with only n.n. bonds are coupled through the diagrams with next-nearest-neighbor (n.n.n.) bonds, as in Figs. 1(f)(ii) and 1(f)(iii). We collectively refer to diagrams with only n.n. and n.n.n. bonds as those with short bonds. There will be considerable pair tunneling in a wave function dominated by VB diagrams with short bonds, and we will refer to such a wave function as a paired-electron liquid (PEL).

*r.t.clay@msstate.edu

†mazumdar@email.arizona.edu

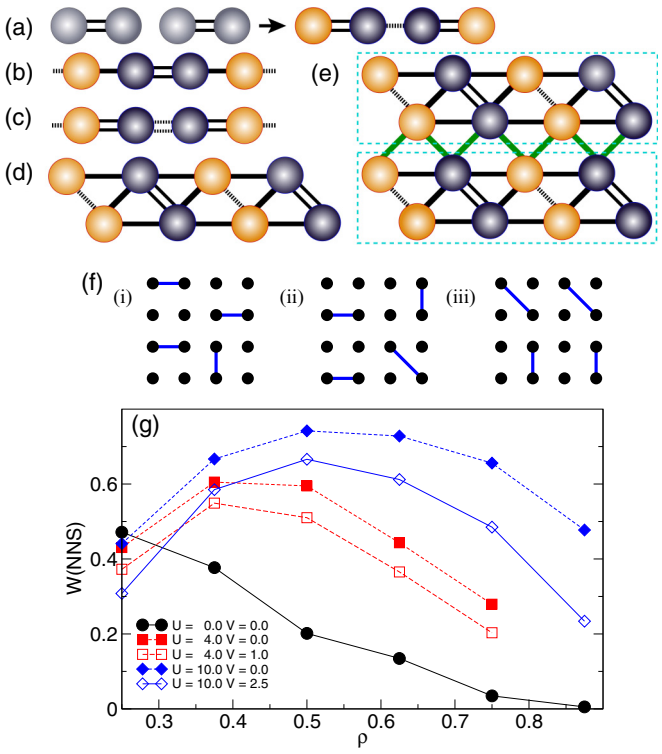

FIG. 1. (a) $\rho = 0.5$ dimers with weak (left) and moderate (right) interdimer singlet bonding. Sites colored gray, blue, and red have charges 0.5, >0.5, and <0.5, respectively. $2k_F$ spin singlet states in the $\rho = 0.5$ 1D chain, for (b) small to intermediate U and V, and (c) for intermediate to large U. In both cases $V < V_c(U)$ [11]. The PEC in the (d) $\rho = 0.5$ zigzag ladder [12], (e) 2D triangular lattice [10]. The CO has pattern . . . 1100 . . . in two directions, where "1" ("0") denote charge-rich (charge-poor) sites. Double, single, and dotted bonds in (b)–(e) denote bonds with decreasing strengths, with the double dotted bond weaker than a single bond but stronger than a single dotted bond. Differences in bond strengths result from nonzero e-p coupling. (f) Covalent VB diagrams with short bonds in $\rho = 0.5$, and (g) their total normalized weights in the ground state wave function of different ρ for the 4×4 lattice, for $t_y = 1$, $t_{x+y} = 0.8$.

In the following section we describe the results of finite-size correlated calculations within Eq. (1) that demonstrate explicitly the enhancement of SC uniquely for $\rho \simeq 0.5$.

II. LATTICES, PARAMETERS, AND RESULTS

We consider an anisotropic triangular lattice with $t_{ij} = \{t_x, t_y, t_{x+y}\}$. We express all quantities with dimensions of energy in units of t_x ($t_x = 1$). The bulk of our calculations are for $t_y \simeq 1$, with t_{x+y} only slightly smaller. This is because antiferromagnetism (AFM) or CO dominate at weaker frustrations [10]. We first calculate the exact wave functions in the lowest total spin $S = 0$ subspace for all ρ within the periodic 4×4 triangular lattice. In Fig. 1(g) we plot the total normalized contribution by the covalent VB diagrams with short bonds to the exact wave function as a function of ρ for several Hubbard U and V. For moderate to large e-e interactions the maximum in this contribution occurs at $\rho = 0.5$, indicating that VB diagrams with short bonds dominate at $\rho = 0.5$.

We anticipate Bose condensation of singlet pairs within the PEL state within the mechanism of SC proposed by Schafroth [14]. Since without e-p coupling in Eq. (1) there is no static SG and PEC, a complete theory of SC will require explicit inclusions of both e-e and dynamic e-p interactions. As is, however, well established from studies of CDWs and SDWs, the *tendency* to the dominant instability in models containing both e-e and e-p interactions can be determined from correlation functions of the electronic Hamiltonian alone [15]. We have performed calculations within Eq. (1) to determine if the dominance of VB diagrams with short bonds at $\rho \simeq 0.5$ implies enhanced superconducting pair correlations. We demonstrate that the PEL is a precursor to a correlated superconducting state.

Our choice of which lattices to consider for calculations of SC pair-pair correlations is guided by several considerations. First, the total number of sites should be less than around 100 in order to obtain accurate results for the pair-pair correlation functions. Second, the lattice should have a single-particle level structure such that quarter-filling ($\rho = 0.5$) is a nondegenerate state, and the L_x and L_y dimensions should be an even number of sites. We took t_x slightly different from t_y ($t_x = 1$, $t_y = 0.9$) in order to maximize the number of densities with nondegenerate single-particle spectra. Within these constraints, and considering only lattices for which $L_y \gtrsim L_x/2$, the only possible choices are 10×10, 10×6, and 6×6. In addition we considered the 4×4 lattice, which although degenerate at $\rho = 0.5$, is the largest lattice for which the full density range can be calculated exactly.

We define the standard singlet pair-creation operators

$$\Delta_i^\dagger = \sum_\nu g(\nu) \frac{1}{\sqrt{2}} (c_{i,\uparrow}^\dagger c_{i+\vec{r}_\nu,\downarrow}^\dagger - c_{i,\downarrow}^\dagger c_{i+\vec{r}_\nu,\uparrow}^\dagger), \qquad (2)$$

where $g(\nu)$ determines the pairing symmetry. The phases $g(\nu)$ determine the pairing symmetry. For $d_{x^2-y^2}$ symmetry, $g(\nu) = \{1,-1,1,-1\}$ for $\vec{r}_\nu = \{\hat{x},\hat{y},-\hat{x},-\hat{y}\}$, respectively. For d_{xy} symmetry, $g(\nu) = \{1,-1,1,-1\}$ for $\vec{r}_\nu = \{\hat{x}+\hat{y},-\hat{x}+\hat{y},-\hat{x}-\hat{y},\hat{x}-\hat{y}\}$, respectively. We note that slightly different definitions of Eq. (2) appear in the literature, in that some definitions do not include the factor of $1/\sqrt{2}$. Caution must therefore be used before comparing directly the magnitude of pair-pair correlations in different references. We calculated equal-time pair-pair correlations $P_{ij} = \langle \Delta_i^\dagger \Delta_j \rangle$, using four different numerical techniques: exact diagonalization in the VB basis [16–18], the path integral renormalization (PIRG) method [19], constrained path Monte Carlo (CPMC) [20], and determinantal quantum Monte Carl (DQMC) [21]. Further details on the methods is given in the Appendix.

To facilitate comparison of multiple lattices and to mitigate finite-size effects, we calculate the distance-dependent pair-pair correlations $P(r)$ ($r \equiv |\vec{r}_i - \vec{r}_j|$) and show here the average long-range pair-pair correlation $\bar{P} = N_P^{-1} \sum_{|\vec{r}|>2} P(r)$, where N_P is the number of terms in the sum [22] (see also Supplemental Material [23], Sec. S.1).

We have found $d_{x^2-y^2}$ and d_{xy} symmetries to dominate over s-wave symmetries. Further, for each lattice only one of the two d-wave channels is relevant; $d_{x^2-y^2}$ for 4×4 and 10×6, and d_{xy} for 6×6 and 10×10 [23]. The origin of this lattice dependence is currently not understood; note, however, that

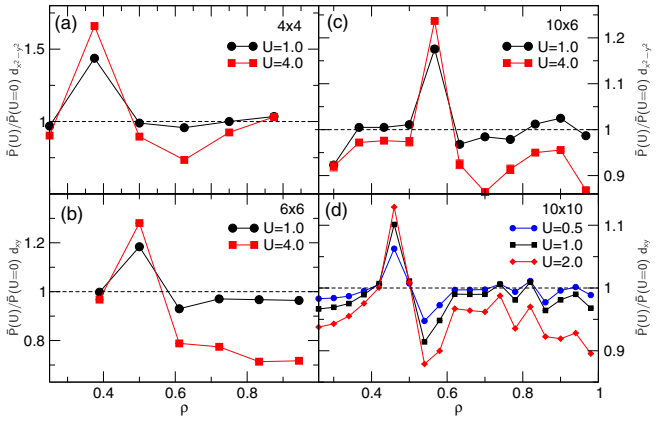

FIG. 2. Average long-range pair-pair correlation $\bar{P}(U)$ normalized by its uncorrelated value for (a) 4×4, (b) 6×6, (c) 10×6, and (d) 10×10 anisotropic triangular lattices, for $t_y = 0.9$ and $t_{x+y} = 0.8$. 4×4 results are exact; 6×6 and 10×6 results are obtained using the PIRG method; and 10×10 by the CPMC method.

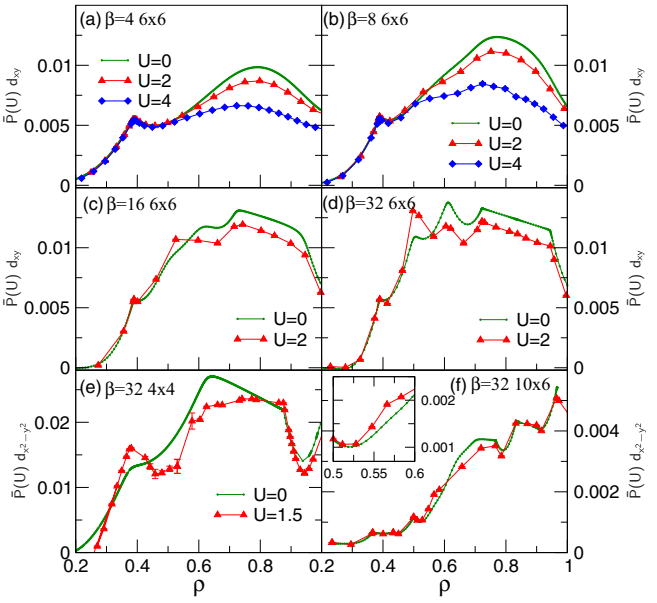

FIG. 3. (a)–(d) $\bar{P}(U)$ for d_{xy} pairing as a function of ρ and inverse temperature β for the 6×6 lattice, calculated using DQMC. $\bar{P}(U)$ for $\rho \simeq 0.5$ is gradually enhanced with increasing β beginning from $\beta = 8$. $\bar{P}(U)$ is suppressed by U at all other ρ. $\bar{P}(U)$ for (e) $d_{x^2-y^2}$ pairing in the 4×4 lattice, and (f) d_{xy} pairing in the 10×6 lattice.

the distinction between $d_{x^2-y^2}$ and d_{xy} symmetries is largely semantic in the strongly frustrated regime we investigate. It is possible that the actual pairing symmetry is a superposition of $d_{x^2-y^2}$ and d_{xy}. We have not attempted to find this superposition. Rather, for each lattice and ρ we have calculated the dominant symmetry $\bar{P}$ as a function of U ($V_{ij} = 0$). Plots of $\bar{P}$ versus U for each individual ρ on different lattices are given in the Supplemental Material [23]. The complete results, summarized in Figs. 2 and 4, are remarkable: For each lattice $\bar{P}(U)/\bar{P}(U = 0) > 1$ for a single ρ that is either exactly 0.5 or one of two closest carrier fillings with closed-shell Fermi-level occupancy at $U = 0$. Pair correlations are suppressed by U at all other ρ, including the region $0.7 < \rho < 1$ that has been extensively investigated [1]. In three of four lattices in Fig. 2 enhancement of $\bar{P}(U)$ occurs for ρ slightly away from 0.5. The magnitude of pair correlations depend on both the pair binding energy and the kinetic energy to be gained from pair delocalization; in finite lattices both quantities depend strongly on the details of the one-electron energy spectrum. We show in the Supplemental Material [23] that the ρ at which enhanced $\bar{P}(U)$ occurs can be predicted from the known one-electron levels. Importantly, the deviation from 0.5 of the ρ at which $\bar{P}(U)$ is enhanced (excluding the 6×6 lattice where this deviation is zero) decreases monotonically with size. SC for ρ close to 1, but U significantly larger than that accessible for our largest lattices ($U \leqslant 4$), has been claimed within approximate calculations [6,24,25]. We discuss ρ close to 1 in the Supplementary Material [23], Sec. S.4, where we show that there exist enough uncertainties here that further work would be needed before firm conclusions can be reached.

Nonzero V_{ij} affects lattice frustration minimally when all three components, V_x, V_y, and V_{x+y} are nonzero. Pair correlations for $V_x = V_y = V_{x+y}$ could be calculated only for the 4×4 lattice, where the behavior of the pair correlations is qualitatively similar to $V_{ij} = 0$, although the magnitude of the enhancement is smaller. We have found that when $V_x = V_y$, $V_{x+y} = 0$, d_{xy} pair correlations are enhanced uniquely for $\rho \simeq 0.5$. Similarly, $V_{x+y} \neq 0$, and any one of V_x, V_y nonzero enhances (suppresses) $d_{x^2-y^2}$ (d_{xy}). Overall, there is a broad parameter region over which the pair correlations remain enhanced at $\rho \simeq 0.5$ (see Supplemental Material [23], Sec. S.1.1).

The ground-state results are further confirmed by finite temperature DQMC calculations. The sign problem is severe for large U, but up to $U = 2$ the results are reliable even for the largest β ($\beta = t_x/k_B T$) we have investigated. Figures 3(a)–3(d) show that with increasing β there occurs progressive enhancement of $\bar{P}(U)$ with increasing U, uniquely at $\rho \simeq 0.5$, in the 6×6 lattice. Figures 3(e) and 3(f) show similar results for the 4×4 and 10×6 lattices. The excellent agreement between PIRG and DQMC indicates that while the DQMC calculations could be performed at the smallest T only for $U \leqslant 2$, enhanced pair correlations should be expected at even larger U. Figure 4 summarizes the enhancement of pairing as a function of ρ for all lattices, including in the nondominant channels. The dominant pairing symmetry is enhanced only for $\rho \simeq 0.5$. Pairing in the nondominant channels is enhanced weakly for small $U \approx 1$ for some ρ, but are weakened further as U is increased.

Despite the large amount of data from our calculations, performing a rigorous finite-size scaling of the pair-pair correlations is difficult for several reasons. First, for the different lattices, the enhancement occurs in either the $d_{x^2-y^2}$ or d_{xy} channels. In the thermodynamic limit the pair symmetry for the highly frustrated lattice we have considered is most likely a superposition of these two symmetries. On finite lattices one or the other tends to dominate. Second, even as the density ρ where enhancement occurs tends to $\rho \approx 0.5$ as the lattice size increases, the precise ρ where the enhancement occurs is different on each lattice. Finally, the CPMC method we used for the 10×10 calculations is approximate, and its accuracy for larger lattices and large U is not known. In our comparison

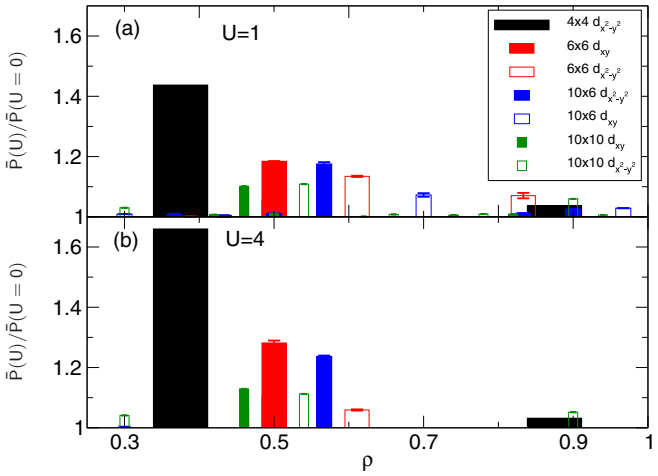

FIG. 4. $\bar{P}(U)$ normalized by $\bar{P}(U=0)$, for (a) $U=1$ and (b) $U=4$ ($U=2$ for the 10×10 lattice). Only results with $\bar{P}(U)/\bar{P}(U=0)>1$ are included, for both $d_{x^2-y^2}$ and d_{xy} pairing symmetries. The dominant pairing symmetry for each lattice is indicated with darker shading. The width of each bar is $1/N$, where N is the number of lattice sites.

of PIRG and CPMC for the 10×6 lattice (see Supplemental Material [23], Fig. S10), CPMC in some cases underestimated $\bar{P}$ for larger U.

Because of these points we cannot make a meaningful extrapolation from a single pairing symmetry at a fixed density. Nevertheless, in Fig. 5 we show our attempt to finite-size scaling of $\bar{P}$ in two different ways, for relatively weak $U=2$. In both panels, *we have taken the density and pairing symmetry where the peak enhancement occurs on each finite lattice.* In Fig. 5(a) we plot the peak value of the ratio $\bar{P}(U)/\bar{P}(U=0)$ as a function of $1/\sqrt{N}$, where N is the total number of lattice sites. Figure 5(b) shows the extrapolation of $\bar{P}(U)$ itself for the same densities as in Fig. 5(a). If superconducting long-range

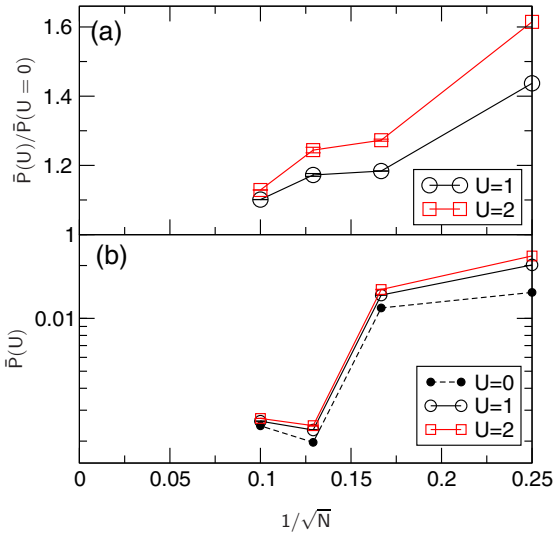

FIG. 5. (a) Finite-size scaling of the $\rho\approx0.5$ peak (see text) $\bar{P}(U)/\bar{P}(U=0)$ for each lattice; (b) Similar scaling plot for $\bar{P}(U)$ at the same densities as in (a).

order is present, $\bar{P}$ should tend to a finite value as the lattice size increases. The data in both Figs. 5(a) and 5(b) appear to indicate absence of long-range order, although we cannot rule out the possibility of a small magnitude ($\bar{P}<0.002$) long-range component in Fig. 5(b). Note also that due to the limitations of CPMC we do not have reliable data for pair correlations at large U ($U>2$) for the 10×10 lattice, where the enhancement would presumably have been larger. If we ignore the $\bar{P}(U)/\bar{P}(U=0)$ for the 10×10 lattice, then the ratio does extrapolate to slightly greater than 1 in Fig. 5(a). This would indicate that the system is indeed a paired-electron liquid state that is *asymptotically close* to a superconducting state with long-range order. We therefore speculate that the inclusion of e-p interactions will give true superconducting long-range order.

III. DISCUSSION

We have demonstrated a completely new source of effective electron-electron attraction, which is mediated by charge-spin coupling (and ultimately also coupling to lattice) at a band-filling far from $\rho=1$. The physical arguments are based on the tendency to charge migration to form nearest-neighbor singlets, which is unique to the $\rho=0.5$ region. The significance of our results lies in the following. (i) This is the first time that consistent enhancement of pair-pair correlations for nonoverlapping pairs [22,26,27] with U is observed. (ii) The enhancement is uniquely at or near $\rho=0.5$, exactly the carrier density where the PEC has been found earlier [10]. (iii) The theory gives consistent explanations of SC as well as many peculiar features observed in the normal states of 2D CTS, as we describe below.

It is highly interesting that superconductivity in the CTS is limited to $\rho\simeq0.5$. While *conducting* charge-transfer solids exist with many other carrier densities there is no example of a superconductor whose carrier density is not exactly or nearly 0.5. Further, our theoretical work is the very first that gives a unified approach to organic superconductivity, independent of whether the ambient pressure proximate semiconductor is magnetic or charge-ordered. We discuss further specific implications for the CTS superconductors below.

Typical quasi-2D superconducting CTS are the families (BEDT-TTF)$_2$X [hereafter (ET)$_2$X], which occur with crystal structures labeled α, β, θ, κ, etc. [28], and Z[Pd(dmit)$_2$]$_2$. The number of holes (electrons) ρ per ET cation [Pd(dmit)$_2$ anion] is 0.5. With the exception of the κ-phase materials (see below), ET molecules occupy the sites of triangular lattices [28]. In many 2D CTS the unit cell consists of two molecules, formally leading to a two- rather than one-band model. In our lattice this would add an additional modulation of the hopping integrals. With strong e-e interactions [29], and the resultant band narrowing effect, the experimental consequence of this modulation is small. For example, due to symmetry the two bands are degenerate in θ-(ET)$_2$X but nondegenerate in α-(ET)$_2$X [30], but similar CO patterns and SC are found in both. SC is reached at constant ρ by application of pressure on a proximate semiconducting state that often exhibits CO. Materials exhibiting CO adjacent to SC include α-(ET)$_2$I$_3$ [31], θ-(ET)$_2$I$_3$ [32], β-(meso-DMBEDT-TTF)$_2$X (X = PF$_6$ and AsF$_6$) [33], and EtMe$_3$P[Pd(dmit)$_2$]$_2$ [34]. In

Sec. S.3 in the Supplemental Material [23], we point out that the CO pattern in the traditional Wigner crystal, driven by large V, is different from that in the PEC [35], where it is driven by the tendency to form n.n. singlets. Experiments have established that the CO pattern in each of the above materials showing CO-to-SC transition corresponds to the PEC [23,33,34,36,37]. The pressure-induced transition to SC in these systems is then likely a bandwidth-driven PEC-to-SC transition suggested from our calculations. A strong role of phonons in SC is seen experimentally [38]. This is expected, as it is the cooperative effect between e-e and e-p interactions [10,11] that drives the transition to the PEC.

Our theory is also applicable to the κ-$(ET)_2X$. At ambient pressure, $X = Cu[N(CN)_2]Cl$ (κ-Cl) is AFM, $X = Cu_2(CN)_3$ (κ-CN) is a quantum spin liquid (QSL), and $X = Cu[N(CN)_2]Br$ (κ-Br) and $X = Cu(NCS)_2$ (κ-NCS) are superconductors [39]. SC is also observed in κ-Cl and κ-CN under pressure [39]. A variety of experiments [40–49] have suggested fluctuating SC and preformed pairs at temperature T^* significantly above the superconducting critical temperature T_c in κ-Br ($T_c = 11.5$ K) and κ-NCS ($T_c = 10.4$ K). While estimates of T^* range from 20 to 50 K, measurements of ESR spin susceptibility [40], static magnetic susceptibility [46], and NMR measurements of spin-lattice relaxation time and Knight shift [41–45] all show a dramatic decrease in magnetic fluctuations and the possible occurrence of a spin gap at T^*. This has been interpreted in terms of incoherent pairs that form at T^* to give fluctuating SC. STM [47] and magnetic torque measurements [48,49] have been interpreted similarly.

In κ-$(ET)_2X$ dimers of ET molecules are arranged on an anisotropic triangular lattice. The underlying monomer lattice is also triangular, albeit distorted [28]. Considering dimers as effective sites gives an effective $\rho = 1$ Hubbard model that yields AFM (QSL) for weak (strong) frustration [39,50]. Precise numerical calculations have however found no SC within the effective $\rho = 1$ Hubbard model for any frustration [26,27,51]. We have shown that with increasing frustration, there is a strong tendency to a fluctuating PEC in κ-$(ET)_2X$, in spite of dimerization [10]. With increased delocalization, dimerization plays a less crucial role and the sites of the lattice are now the monomer molecules themselves [10]. Strong support for this theoretical picture is obtained from the observations of the PEC in κ-$(ET)_2Hg(SCN)_2Cl$ [52], and of a pressure-induced transition from a dimer AFM to a state with significant intradimer charge fluctuation in β'-$(ET)_2$-ICl_2 [53]. Taken together with earlier work [10], our present work is then able to explain both the magnetic behavior and SC: in the localized insulating phase dimerization plays a deciding role and the effective $\rho = 1$ description is valid; with pressure-induced larger interdimer hopping, the effective picture breaks down and a more appropriate description is $\rho = 0.5$. Within our theory the state below T^* is the PEL, which is the fluctuating SC state observed experimentally [40–49], and which is superconducting once pair coherence is reached. In Fig. 3, enhanced pair correlation at $\rho = 0.5$ begins to appear at $\beta = 8$; with average $|t| \sim 0.1$ eV, T^* can be as high as ~ 100 K, which is to be compared with experimental estimates of $T^* \sim 50$ K [40–44]. Lattice effects in the transition at T^* have been found in ultrasound [54] and thermal expansion [55] studies. This is expected, since the PEL is structurally close to the PEC, a density wave of pairs [10].

IV. CONCLUSION

To summarize, we have shown that there occurs a coupled charge-spin-mediated effective e-e attraction near $\rho = 0.5$ because of the strong tendency to form n.n. singlets at this density. Two of us have pointed out the unusual abundance [56] of correlated-electron superconductors at $\rho \simeq 0.5$. It is conceivable that the shared features of $\rho = 0.5$, lattice frustration, and strong e-e interaction point to a new paradigm for correlated-electron SC. Recent finding of a CO phase proximate to SC within the pseudogap phase of the cuprates [57–60] has led to theories of competing or intertwined CO and SC orders. Whether or not the PEC to PEL transition found by us has any bearing here too is an intriguing question.

ACKNOWLEDGMENTS

This work was supported by the U.S. Department of Energy Grant No. DE-FG02-06ER46315 (De Silva, Dutta, and Clay) and by the U.S. National Science Foundation Grant No. NSF-CHE-1151475 (Gomes and Mazumdar). Part of the calculations were performed using resources of the National Energy Research Scientific Computing Center (NERSC), which is supported by the Office of Science of the U.S. Department of Energy under Contract No. DE-AC02-05CH11231. We thank Prof. David K. Campbell and Prof. Charles Stafford for their critical reading of the manuscript and helpful comments.

APPENDIX: METHODS

Exact diagonalization using the valence-bond basis. The valence-bond method is a well-known numerical technique for studying correlated quantum systems [16–18]. In the present work it is used for computing pair-pair correlation functions and relative weights of nearest- and next-nearest-neighbor VB diagrams for the 4×4 lattice. In the VB method [16–18], the wave function is expanded in terms of VB diagrams $|\phi_n\rangle$:

$$|\Psi\rangle = \sum_n c_n |\phi_n\rangle. \tag{A1}$$

As the VB basis is nonorthogonal the normalization condition involves the overlap of VB diagrams, $\langle\phi_n|\phi_m\rangle$:

$$\langle\Psi|\Psi\rangle = \sum_{m,n} c_n^\star c_m \langle\phi_n|\phi_m\rangle. \tag{A2}$$

In Fig. 1(g) we plot the total relative weight of nearest- and next-nearest-neighbor singlet VB diagrams, $W(NNS)$. This quantity is defined as

$$W(NNS) = \sum_{m,n}{}' c_n^* c_m \langle\phi_n \mid \phi_m\rangle / \langle\Psi|\Psi\rangle. \tag{A3}$$

In Eq. (5), the $'$ over the sum indicates that only VB diagrams with either nearest- or next-nearest-neighbor singlet bonds are included [as shown, for example, in Fig. 1(f)].

The main advantages of the the VB method are that it allows, first, visualization of wave functions in terms of the dominant VB diagrams, and second, conservation of total spin S. We have used this method to calculate correlation functions for the 4×4 lattice within the lowest $S = 0$ state for all values of t_{x+y}; for number of electrons 4, 8, and 12, the single-particle wave functions are degenerate, and for these cases calculations targeting specific total S states would be difficult for methods conserving only S_z.

Path integral renormalization group. PIRG was used to calculate zero-temperature expectation values of the pair-pair correlations. PIRG was used because conventional Monte Carlo methods (see below) are limited by the fermion sign problem to either small Hubbard U and/or high temperatures for frustrated lattices. The PIRG method is described in Ref. [19]. Within PIRG, the wave function is expanded as a sum over L Slater determinants, and the projector operator $\exp(-\tau H)$ is used to project out the ground state from a random starting determinant [19]. The method is exact at $U = 0$ and for each L, PIRG calculations are variational. For the calculations presented here, we first minimized the variational energy for $L = 1$, followed by optimizing the variational state at $L = 8$. We then continued calculations to larger L, doubling ($L = 16, 32, \ldots$) L at each step. We used maximum L's of up to 768. The finite-basis bias is then removed by extrapolating quantities as a function of the energy variance ΔE [19]. For the results presented here, we typically used a linear extrapolation in ΔE for the three largest L used, i.e., $L = \{256, 512, 768\}$.

Several additional techniques are essential to improve the accuracy of the PIRG. First, we incorporated lattice and spin symmetries using projection operators of the QP-PIRG method of Ref. [61]. The use of lattice and spin symmetries has been shown to drastically reduce the L required to obtain accurate results with PIRG [61]. Here we used the more accurate method of incorporating symmetries during projection (QP-PIRG) as opposed to afterwards (PIRG-QP) [61]. For the lattice symmetry we used the full space group of the lattice (translations and point symmetries). For spin, we projected using the spin-parity operator, which separates even and odd values of total spin S. All results here are for the even spin-parity subspace. Second, it has been observed that in certain cases the PIRG method can be trapped in excited states [62]. To help prevent this, in addition to the PIRG projection operator, we used a random simulated annealing-like modification of the Slater determinants [27,62]. Furthermore, several starting states were chosen for the projection, and their final energy compared.

PIRG has been extensively benchmarked against other methods. We previously compared the pair-pair correlations from PIRG and exact diagonalization on a 4×4 frustrated lattice and found essentially perfect agreement [27]. For larger lattices, PIRG has further been checked against conventional quantum Monte Carlo for systems where there is no sign problem, such as the half-filled square lattice Hubbard model [61]. Our comparisons of PIRG and DQMC (see Supplemental Material Sec. S.1 [23]) further gives us confidence in the accuracy of the method.

Constrained path Monte Carlo. CPMC is a ground-state projector QMC method [20]. Like PIRG, CPMC works in the space of Slater determinants. This space is over-complete, which results in contributions to the ground-state wave function that are both positive and negative. The Monte Carlo sampling is confined to the region where the overlap between each random walker $|\phi\rangle$ and a trial wave function $|\Psi_T\rangle$ is positive [20]. This eliminates the loss of precision known as the fermion sign problem but introduces an approximation into the method. The results presented here used the free-electron wave function for $|\Psi_T\rangle$. This trial function produces exact CPMC results at $U = 0$ and also for nonzero U in the one-dimensional limit [20]. While this choice has been shown to be accurate for many lattices, particularly for closed-shell fillings [20], we restrict the use of CPMC to small U ($0 < U \lesssim 2$). Our CPMC code results used an imaginary time discretization of $\Delta\tau = 0.1$ with a second-order Trotter approximation; the additional systematic error due to this approximation is negligible.

Determinantal quantum Monte Carlo. The DQMC method integrates out the fermion degrees of freedom, replacing the Hubbard interaction with an auxiliary Hubbard-Stratonovich field [21]; for a review see Ref. [63]. Our results here used the finite-temperature variant of this algorithm. This method suffers from sign problem when used for fermion systems. As shown in Fig. 3, in the 6×6 lattice an inverse temperature of at least $\beta \approx 8$ is required to see the enhancement of pairing at $\rho \simeq 0.5$. At these lower temperatures, the sign problem limits us to $U \approx 2$. Our results used a Trotter discretization in imaginary time of $\Delta\tau = 0.1$; for $U = 2$ the systematic error due to this approximation is smaller than the point size on our plots and can be neglected.

[1] D. J. Scalapino, Rev. Mod. Phys. **84**, 1383 (2012).
[2] S. R. White, D. J. Scalapino, R. L. Sugar, N. E. Bickers, and R. T. Scalettar, Phys. Rev. B **39**, R839 (1989).
[3] S. Zhang, J. Carlson, and J. E. Gubernatis, Phys. Rev. Lett. **78**, 4486 (1997).
[4] E. Dagotto, Rev. Mod. Phys. **66**, 763 (1994).
[5] M. Guerrero, G. Ortiz, and J. E. Gubernatis, Phys. Rev. B **59**, 1706 (1999).
[6] T. Misawa and M. Imada, Phys. Rev. B **90**, 115137 (2014).
[7] M. Troyer, H. Tsunetsugu, and T. M. Rice, Phys. Rev. B **53**, 251 (1996).
[8] E. Arrigoni, E. Fradkin, and S. A. Kivelson, Phys. Rev. B **69**, 214519 (2004).
[9] T. Ishiguro, K. Yamaji, and G. Saito, *Organic Superconductors* (Springer-Verlag, New York, 1998).
[10] S. Dayal, R. T. Clay, H. Li, and S. Mazumdar, Phys. Rev. B **83**, 245106 (2011).
[11] R. T. Clay, S. Mazumdar, and D. K. Campbell, Phys. Rev. B **67**, 115121 (2003).
[12] R. T. Clay and S. Mazumdar, Phys. Rev. Lett. **94**, 207206 (2005).
[13] P. W. Anderson, Science **235**, 1196 (1987).
[14] M. R. Schafroth, Phys. Rev. **100**, 463 (1955).

[15] J. E. Hirsch and D. J. Scalapino, Phys. Rev. B **29**, 5554 (1984).
[16] Z. G. Soos and S. Ramasesha, Phys. Rev. B **29**, 5410 (1984).
[17] S. Ramasesha and Z. G. Soos, Int. J. Quant. Chem. **25**, 1003 (1984).
[18] S. Ramasesha, Chem. Phys. Lett. **130**, 522 (1986).
[19] T. Kashima and M. Imada, J. Phys. Soc. Jpn. **70**, 2287 (2001).
[20] S. Zhang, J. Carlson, and J. E. Gubernatis, Phys. Rev. B **55**, 7464 (1997).
[21] R. Blankenbecler, D. J. Scalapino, and R. L. Sugar, Phys. Rev. D **24**, 2278 (1981).
[22] Z. B. Huang, H. Q. Lin, and J. E. Gubernatis, Phys. Rev. B **64**, 205101 (2001).
[23] See Supplemental Material at http://link.aps.org/supplemental/10.1103/PhysRevB.93.165110 for the full U-dependence of the data presented in Sec. II.
[24] E. Gull, O. Parcollet, and A. J. Millis, Phys. Rev. Lett. **110**, 216405 (2013).
[25] H. Yokoyama, M. Ogata, Y. Tanaka, K. Kobayashi, and H. Tsuchiura, J. Phys. Soc. Jpn. **82**, 014707 (2013).
[26] R. T. Clay, H. Li, and S. Mazumdar, Phys. Rev. Lett. **101**, 166403 (2008).
[27] S. Dayal, R. T. Clay, and S. Mazumdar, Phys. Rev. B **85**, 165141 (2012).
[28] H. Mori, J. Phys. Soc. Jpn. **75**, 051003 (2006).
[29] H. Kino and H. Fukuyama, J. Phys. Soc. Jpn. **64**, 2726 (1995).
[30] T. Mori, H. Mori, and S. Tanaka, Bull. Chem. Soc. Jpn. **72**, 179 (1999).
[31] N. Tajima *et al.*, J. Phys. Soc. Jpn. **75**, 051010 (2006).
[32] H. Kobayashi, A. Kobayashi, and R. Kato, Solid State Phys. **21**, 826 (1986).
[33] T. Shikama *et al.*, Crystals **2**, 1502 (2012).
[34] M. Tamura, A. Nakao, and R. Kato, J. Phys. Soc. Jpn. **75**, 093701 (2006).
[35] R. T. Clay, S. Mazumdar, and D. K. Campbell, J. Phys. Soc. Jpn. **71**, 1816 (2002).
[36] T. Ivek, B. Korin-Hamzic, O. Milat, S. Tomic, C. Clauss, N. Drichko, D. Schweitzer, and M. Dressel, Phys. Rev. B **83**, 165128 (2011).
[37] M. Watanabe, Y. Noda, Y. Nogami, and H. Mori, J. Phys. Soc. Jpn. **76**, 124602 (2007).
[38] A. Girlando, M. Masino, A. Brillante, R. G. DellaValle, and E. Venuti, Phys. Rev. B **66**, 100507(R) (2002).
[39] K. Kanoda and R. Kato, Annu. Rev. Condens. Matter Phys. **2**, 167 (2011).
[40] V. Kataev, G. Winkel, D. Khomskii, D. Wohllenben, W. Crump, K. F. Tebbe, and J. Hahn, Solid St. Comm. **83**, 435 (1992).
[41] H. Mayaffre, P. Wzietek, C. Lenoir, D. D. Jérome, and P. Batail, Europhys. Lett. **28**, 205 (1994).
[42] S. M. De Soto, C. P. Slichter, A. M. Kini, H. H. Wang, U. Geiser, and J. M. Williams, Phys. Rev. B **52**, 10364 (1995).
[43] A. Kawamoto, K. Miyagawa, Y. Nakazawa, and K. Kanoda, Phys. Rev. Lett. **74**, 3455 (1995).
[44] M. Itaya, Y. Eto, A. Kawamoto, and H. Taniguchi, Phys. Rev. Lett. **102**, 227003 (2009).
[45] T. Kobayashi, Y. Ihara, Y. Saito, and A. Kawamoto, Phys. Rev. B **89**, 165141 (2014).
[46] T. Uehara, M. Ito, H. Taniguchi, and K. Satoh, J. Phys. Soc. Jpn. **82**, 073706 (2013).
[47] T. Arai, K. Ichimura, K. Nomura, S. Takasaki, J. Yamada, S. Nakatsuji, and H. Anzai, Solid St. Comm. **116**, 679 (2000).
[48] S. Tsuchiya, J. I. Yamada, S. Tanda, K. Ichimura, T. Terashima, N. Kurita, K. Kodama, and S. Uji, Phys. Rev. B **85**, 220506(R) (2012).
[49] S. Tsuchiya, J. Yamada, T. Terashima, N. Kurita, K. Kodama, K. Sugii, and S. Uji, J. Phys. Soc. Jpn. **82**, 064711 (2013).
[50] B. J. Powell and R. H. McKenzie, Rep. Progr. Phys. **74**, 056501 (2011).
[51] L. F. Tocchio, A. Parola, C. Gros, and F. Becca, Phys. Rev. B **80**, 064419 (2009).
[52] N. Drichko, R. Beyer, E. Rose, M. Dressel, J. A. Schlueter, S. A. Turunova, E. I. Zhilyaeva, and R. N. Lyubovskaya, Phys. Rev. B **89**, 075133 (2014).
[53] K. Hashimoto, R. Kobayashi, H. Okamura, H. Taniguchi, Y. Ikemoto, T. Moriwaki, S. Iguchi, M. Naka, S. Ishihara, and T. Sasaki, Phys. Rev. B **92**, 085149 (2015).
[54] K. Frikach, M. Poirier, M. Castonguay, and K. D. Truong, Phys. Rev. B **61**, R6491 (2000).
[55] J. Müller, M. Lang, F. Steglich, J. A. Schlueter, A. M. Kini, and T. Sasaki, Phys. Rev. B **65**, 144521 (2002).
[56] S. Mazumdar and R. T. Clay, Int. J. Quant. Chem. **114**, 1053 (2014).
[57] R. Comin *et al.*, Science **343**, 390 (2014).
[58] E. H. D. S. Neto *et al.*, Science **343**, 393 (2014).
[59] E. H. D. S. Neto *et al.*, Science **347**, 282 (2015).
[60] T. Wu *et al.*, Nat. Commun. **6**, 6438 (2015).
[61] T. Mizusaki and M. Imada, Phys. Rev. B **69**, 125110 (2004).
[62] T. Yoshioka, A. Koga, and N. Kawakami, J. Phys. Soc. Jpn. **77**, 104702 (2008).
[63] E. Y. Loh, Jr. and J. E. Gubernatis, in *Electronic Phase Transitions*, edited by W. Hanke and Yu. V. Kopaev (Elsevier, Amsterdam, 1992), pp. 177–235.